
Prior Activation Distribution (PAD): A Versatile Representation to Utilize DNN Hidden Units

Lakmal Meegahapola
EPFL & Idiap Research Institute
Switzerland
lakmal.meegahapola@epfl.ch

Vengateswaran Subramaniam
Singapore Management University
Singapore
vengates@smu.edu.sg

Lance Kaplan
U.S. Army Research Laboratory
USA
lance.m.kaplan.civ@mail.mil

Archan Misra
Singapore Management University
Singapore
archanm@smu.edu.sg

Abstract

In this paper, we introduce the concept of Prior Activation Distribution (PAD) as a versatile and general technique to capture the typical activation patterns of hidden layer units of a Deep Neural Network used for classification tasks. We show that the combined neural activations of such a hidden layer have class-specific distributional properties, and then define multiple statistical measures to compute how far a test sample’s activations deviate from such distributions. Using a variety of benchmark datasets (including MNIST, CIFAR10, Fashion-MNIST & notMNIST), we show how such PAD-based measures can be used, independent of any training technique, to (a) derive fine-grained uncertainty estimates for inferences; (b) provide inferencing accuracy competitive with alternatives that require execution of the full pipeline, and (c) reliably isolate out-of-distribution test samples.

1 Introduction

Deep Neural Networks (DNNs) [26] have rapidly become an indispensable mechanism for implementing machine intelligence for a variety of tasks, such as medical image analysis [28], chatbots for conversational interactions [19] and navigation of autonomous vehicles & robots [38, 39, 9]. DNNs represent state-of-the-art techniques for multi-class classification problems, which conventionally use the point estimates of the final softmax layer to identify the class with the highest confidence value.

DNNs are still largely viewed as “black box” models that generate inferences—a significant amount of ongoing research focuses on improving their *final-layer* accuracy, often by increasing the depth of the inferencing pipeline (e.g., Resnet [16] with 152 layers). With a few notable exceptions (e.g., [1, 51, 5]), researchers have typically not devoted much systematic attention to characterizing or exploiting the activation values of intermediate, *hidden* layers. In this work, inspired by the work of Alain & Bengio [1] in understanding hidden DNN layers, we “unpack” this black box and propose the novel concept of *Prior Activation Distribution (PAD)* as a fundamental construct for characterizing DNNs. PAD specifically focuses on the *activation values* associated with hidden units (e.g., dense neurons, flattened convolutional layers, pooling layer values), and uses *aggregated, statistical* properties of such activation values as a formal mechanism to tackle a variety of DNN-related problems.

We initially developed the PAD construct to quantify the *predictive uncertainty* associated with DNN inferences. It is known that the confidence values of the softmax layer alone do not capture

the uncertainty of the underlying inferencing process [35, 11, 23]. Recently proposed Bayesian Deep Learning (BDL) approaches [31, 30] can model such DNN uncertainty in a more theoretically-grounded manner, but impose significant computational complexity in both training and inference [11]. Moreover, softmax-based inferences require the execution of the entire DNN pipeline, which may impose high latency when executed on resource-limited embedded platforms. We shall show that PAD serves as a *versatile, computationally-inexpensive* way to quantify such uncertainty: PAD makes no assumption on the training mechanism and can be applied independent of the choice of regularization techniques (e.g., dropout, batch normalization, data augmentation). In addition, we provide evidence that (a) PAD-based uncertainty measures may enable more reliable filtering of out-of-distribution (OOD) data without compromising the base classification accuracy, and (b) the use of PADs may enable us to achieve competitive accuracy while only partially executing the DNN pipeline.

1.1 Hypothesis and Contribution

Our hypothesis is that, given any existing (trained) DNN model, the activation values of each hidden unit of a DNN contain *latent* information, that makes it more or less likely to be generated by a member of a specific class. By collecting the activation values from all training instances of a specific class, we can then create an appropriate, *per-class*, representation of the *typical range, or distribution* of each neuron’s values. When making inferences (on a test sample), we posit that the larger the deviation of a hidden unit’s activation value from this typical range, for a specific class, the lower the likelihood that the sample belongs to this class. By aggregating such deviation scores (through appropriate statistical features) across all the neurons in an hidden layer, we believe that we can better quantify the test sample’s likelihood of belonging to this class. Overall, PADs allow us to analyze DNNs by understanding the behavior of neurons in hidden layers, which we believe represents a step towards the goals of making deep learning models more uncertainty-aware, less computationally complex and more interpretable. PADs also provide attestation to our belief that exploiting the behavior of hidden layers can help build richer models of DNN behavior than possible solely from output layer observations.

Key Contributions: We highlight the following key contributions:

- We introduce the novel concept of Prior Activation Distribution (PAD), a simple technique to model hidden-unit activations of a DNN in multi-class classification problems. Further, we empirically demonstrate that PADs can be utilized to model different types of layers, regardless of the model architecture or regularization techniques used. We also develop statistical measures, over PAD values, that help represent such hidden unit behavior.
- We empirically demonstrate that PADs can capture and quantify the "Predictive Uncertainty" associated with a classification output. PAD-based uncertainty measures correspond closely to alternative, more complex models for uncertainty computation.
- We show that, by using additional PAD-based features in conjunction with conventional output confidence scores, DNN classifiers can robustly identify and discard out-of-distribution (OOD) test samples, without sacrificing the ability to reliably classify in-distribution samples. We also provide early empirical evidence that PADs can be leveraged on to provide high classification accuracy, without executing the entirety of a DNN pipeline.

2 Proposed Approach

2.1 Formulating the Hidden Units of Hidden Layers

Let’s consider a trained DNN model \mathbf{G} for a $|C|$ -class classification problem, which has been trained using training data $\mathbf{X}_{train} = \{\mathbf{x}_1, \mathbf{x}_2, \dots, \mathbf{x}_m\}$ and training labels $\mathbf{Y}_{train} = \{\mathbf{y}_1, \mathbf{y}_2, \dots, \mathbf{y}_m\}$ where m is the training dataset size and C denotes the set of class labels. Let $\mathbf{Y}_{train}^{out} = \{\mathbf{y}_1^{out}, \mathbf{y}_2^{out}, \dots, \mathbf{y}_m^{out}\}$ be the set of output labels, when evaluated on the \mathbf{X}_{train} it self. The convention is to calculate training accuracy using the instances where $\mathbf{y}_i^{out} = \mathbf{y}_i$ where $\mathbf{y}_i^{out} \in \mathbf{Y}_{train}^{out}$, $\mathbf{y}_i \in \mathbf{Y}_{train}$ and $i \in [1, \mathbf{m}]$.

Consider a \mathbf{G} , with a set of layers $\mathbf{L} = \{\mathbf{l}_1, \mathbf{l}_2, \dots, \mathbf{l}_p\}$, such that the number of hidden units in each layer be denoted by the set $\mathbf{S} = \{\mathbf{s}_1, \mathbf{s}_2, \dots, \mathbf{s}_p\}$, where p = number of hidden layers. We can represent activation of a hidden unit \mathbf{a}_i in a particular layer \mathbf{l}_j as $\alpha_{\mathbf{a}_i}^{\mathbf{l}_j}$ where $\mathbf{l}_j \in \mathbf{L}$, $\mathbf{a}_i \in [1, \mathbf{s}_j]$, $\mathbf{s}_j \in \mathbf{S}$. Here,

s_j represents the number of hidden units in the layer \mathbf{I}_j . To avoid ambiguity, we positionally index layers from beginning to the end (thus \mathbf{I}_1 represents the input layer), and the hidden-units from top to bottom (thus a_1^j represents the top-most neuron in the j^{th} layer).

Extending this terminology, we define $\alpha_{\mathbf{a}_j, \mathbf{c}_t}^{l_i, \mathbf{x}_e}$ where activation of a hidden unit with (1) positional index $\mathbf{a}_j \in [1, s_j]$ in layer $\mathbf{I}_i \in \mathbf{L}$, when (2) the input to \mathbf{G} is $\mathbf{x}_e \in \mathbf{X}_{\text{train}}$, and (3) output of the network is **correct**, and (4) it belongs to class $\mathbf{c}_t \in \mathbf{C}$. Here $\mathbf{C} = \{\mathbf{c}_1, \mathbf{c}_2, \dots, \mathbf{c}_n\}$ is the set of classification outputs. When $\mathbf{X}_{\text{train}}$ is used, with 1 stochastic forward pass of each $\mathbf{x}_e \in \mathbf{X}_{\text{train}}$ through model \mathbf{G} , using the above definitions, we are able to obtain a distribution of activations, *for each class, for each hidden unit*. We refer to this set of distributions, as the *Prior Activation Distribution (PAD)*.

We make the following two important observations: (a) *Independent of Learning Technique*: The PAD distributions are derived merely by passing the elements of the training dataset through an *already trained DNN*—the definition of PAD is thus agnostic to the choice of training methods and parameters; (b) *Utilizes Correct Classifications only*: Only training instances that are correctly classified contribute to the PAD model. This makes intuitive sense: PAD is used to represent the distribution of neural behavior observed, per class, only when the model is accurate.

For a hidden unit in the positional index of \mathbf{a} in layer \mathbf{I} , **PAD** can be denoted using the notation;

$$\mathbf{PAD} = \{\mathbf{D}(\mu_{a, c_1}^l, \sigma_{a, c_1}^l), \mathbf{D}(\mu_{a, c_2}^l, \sigma_{a, c_2}^l), \dots, \mathbf{D}(\mu_{a, c_n}^l, \sigma_{a, c_n}^l)\} \quad (1)$$

$$\mu_{a, c_t}^l = \frac{\sum \alpha_{a, c_t}^{l, x_e}}{\text{count}_{c_t}} \quad \text{and} \quad \sigma_{a, c_t}^l = \sqrt{\frac{\sum (\alpha_{a, c_t}^{l, x_e} - \mu_{a, c_t}^l)^2}{\text{count}_{c_t}}} \quad \text{where } \mathbf{c}_t \in \mathbf{C}, \mathbf{x}_e \in \mathbf{X}_{\text{train}} \quad (2)$$

In this definition, \mathbf{D} denotes any arbitrary empirical distribution, count_{c_t} is the number of accurate inferences for \mathbf{x}_e which outputs a particular class \mathbf{c}_t . As suggested by our hypothesis, the above definitions allow us to model each hidden unit as a PAD which consists of several distributions, each of which characterize how the hidden-unit activations should behave to produce a particular classification ($\mathbf{c}_t \in \mathbf{C}$). Note also that we make no distributional assumptions (e.g., Gaussian, often used in prior work [11, 13, 18, 36]) on \mathbf{D} ; in Section 3.1, we shall see that these values are, in fact, quite arbitrary.

2.2 Inference Using PADs: KL-divergence Z-Score metrics

We now describe how statistical properties of such distributions are used to evaluate the ‘fit to a specific class’ of a test sample during the inferencing phase. After choosing a particular layer \mathbf{I} which we want to model with **PADs**, we obtain PADs for all hidden-units in \mathbf{I} using the training dataset, denoted by $\mathbf{priors}_l = \{\mathbf{PAD}_1, \mathbf{PAD}_2, \dots, \mathbf{PAD}_s\}$. During the inferencing process, the test sample **input**_{test} is passed through the DNN and generates a set of s_l activation values (one for each hidden unit), in addition to the output prediction (at the final softmax layer) by the DNN. Let us denote these activation values layer \mathbf{I} with s hidden units as **activations**_{test} = $\{\gamma_1, \gamma_2, \dots, \gamma_s\}$. We then propose the following 2 representative statistical features to capture the similarity (or divergence) between the activation firings represented by PAD and those resulting from the test instance: (a) the *KL-score* feature looks at the activation values across all hidden units of a layer jointly, while (b) the *Z-score* feature first measures per-hidden unit divergence in activation values before aggregating across all hidden units.

2.2.1 KL-Score Metric

At a high-level, the KL-Score considers the set of individual activation values of a layer as a whole—i.e., as a s dimensional vector, and compares the test-instance vector against each of the $|C|$ PAD-based vectors. More specifically, for a layer \mathbf{I} with s nodes, the PAD vector for a class c_t consists of s elements, where the a^{th} element is obtained by taking the *mean* value of the activation values μ_{a, c_t}^l . The distance between the test instance and class c_t is computed by the KL-divergence of the normalized values of **activations**_{test} and the activation vector for class c_t . In this fashion, one can compute the overall KL-divergence vector $kl\text{scores}^l$, whose elements consist of the KL-divergence measure for each of the $n = |C|$ classes—i.e., $\mathbf{kl\text{scores}}^l = \{kl\text{score}_{c_1}, kl\text{score}_{c_2}, \dots, kl\text{score}_{c_n}\}$.

Dataset	Model Summary	Training Testing Split	Regularization techniques	Optimizer	Reference
MNIST	C32, D128, D10	60000-10000	Dropout	adam	MA1
MNIST	C64, C128, D128, D10 (Modified LeNet-5 [27])	60000-10000	Dropout	adam	MA2
MNIST	C32, C64, D128, D10 [8]	60000-10000	Dropout	adam	MA3
CIFAR10	C32, C32, C64, C64, D512, D10 [7]	50000-10000	Dropout	adam	CA1
CIFAR10	Modified All Convolutional Net [43, 22]	50000-10000	Batch Normalization, Dropout	RMS(learning rate = 0.01, decay = 1e-6)	CA2
CIFAR10	All Convolutional Net [43]	50000-10000	Data Augmentation	SGD(learning rate = 0.01, decay = 1e-6)	CA3
Fashion-MNIST	C64, C32, D256, D10 [32]	60000-10000	Dropout	adam	FMA1
NotMNIST	-	NA-100000	-	-	NM1
Modified-MNIST	-	NA-10000	-	-	MM1

Table 1: Summary of the datasets and model architectures. The notation uses C, D to represent Conv2D & Dense units respectively, while the subsequent number specifies the number of hidden-units:e.g., D128 represents a layer with 128 dense neurons.

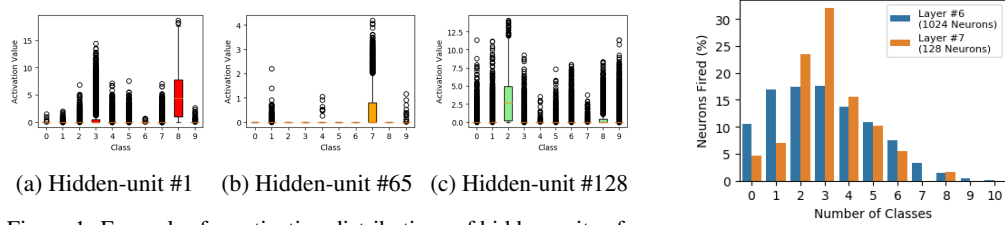


Figure 1: Examples for activation distributions of hidden-units of a DNN trained for MNIST dataset. The hidden-units here are from a Figure 2: Histogram of number of classes against fired neurons percentage

Given this formulation, the higher the KL-score, the lower the likelihood of a test instance belong to that class. Accordingly, to classify the test sample using just the KL-score values at hidden layer l , we would generate an output corresponding to $\min(\mathbf{klscores}^l)$.

2.2.2 Z-score Metric

This approach first looks at each (hidden,class) individually and computes a Z-score¹, representing the degree to which the test sample’s activation value can be considered an outlier, given the representative mean (μ_{a,c_t}^l) and standard deviation (σ_{a,c_t}^l). When $n = |C|$, this pseudoZ-score, across all classes, but for neuron a in hidden layer l , is first computed as: $\mathbf{zscores}_a^l = \left\{ \frac{\gamma_a - \mu_{a,c_1}^l}{\sigma_{a,c_1}^l}, \frac{\gamma_a - \mu_{a,c_2}^l}{\sigma_{a,c_2}^l}, \dots, \frac{\gamma_a - \mu_{a,c_n}^l}{\sigma_{a,c_n}^l} \right\}$.

Subsequently, the Z-score $zscores^l$, across all the s_l neurons in layer l , is computed as the mean of these s_l distinct values, defined as:

$$\begin{aligned} \mathbf{zscores}^l &= \left\{ \frac{\sum_{a=1}^s \frac{\gamma_a - \mu_{a,c_1}^l}{\sigma_{a,c_1}^l}}{s}, \frac{\sum_{a=1}^s \frac{\gamma_a - \mu_{a,c_2}^l}{\sigma_{a,c_2}^l}}{s}, \dots, \frac{\sum_{a=1}^s \frac{\gamma_a - \mu_{a,c_n}^l}{\sigma_{a,c_n}^l}}{s} \right\} \\ &= \{zscore_{c_1}, zscore_{c_2}, \dots, zscore_{c_n}\} \end{aligned} \quad (3)$$

Given this formulation, the *higher* the Z-score, the lower the likelihood of a test instance belonging to that class. Accordingly, to classify the test sample using the observed activations at hidden layer l , we would generate an output corresponding to $\min(\mathbf{zscores}^l)$.

3 Preliminary Analysis

In this section and section 4, we extensively analyze the properties of PAD (and the related *KL* and *Z-score* features), using multiple benchmark classification datasets: MNIST [27], CIFAR10 [21], Fashion-MNIST [49], notMNIST [4], Modified-MNIST² datasets. All the experiments were implemented and evaluated using Python [46] with Keras library [6] with a Tensorflow [10] backend. All the model configurations we used are summarized in Table 1.

3.1 Behavior of Hidden-Layer Activations of DNNs

We carried out several preliminary experiments to understand the behavior of hidden layer activations. We will use the following example to illustrate our findings. We trained a DNN for MNIST dataset

¹Technically, this is a *pseudo* Z-score, at it does measure the distance of a data point (in terms of the number of standard deviations) from the mean, but does not assume a Normal distribution.

²Modified MNIST dataset was created by combining pairs of consecutive images of MNIST. A sample from this dataset is shown in 4

Example	KL-scores Z-scores	Softmax Output	min of KL	min of Z-scores	Ground truth
Figure 3a	{2.223, 1.627, 1.653, 1.599, 1.539, 1.364, 1.073 , 1.169, 1.181, 1.239} {1.987, 1.147, 1.062, 0.975, 0.881, 0.733, 0.594 , 0.633, 0.636, 0.657}	6 (98%)	6	6	6
Figure 3b	{2.445, 2.038, 2.08, 1.566, 1.442, 1.207, 1.269, 1.188, 1.183 , 1.125} {1.951, 1.321, 1.224, 0.877, 0.702, 0.58, 0.600, 0.567, 0.566 , 0.547}	5 (78%)	9	9	9
Figure 3c	{2.465, 1.335 , 3.798, 3.483, 4.373, 4.006, 3.849, 4.244, 1.396, 1.454} {1.951, 1.321, 1.224, 0.877, 0.702, 0.58, 0.600, 0.567, 0.566 , 0.547 }	ship (76.5%)	automobile	truck	automobile
Figure 3d	{2.223, 1.627, 1.653, 1.599, 1.539, 1.364, 1.073 , 1.169, 1.181, 1.239} {1.987, 1.147, 1.062, 0.975, 0.881, 0.733, 0.594 , 0.633, 0.636, 0.657}	truck (73.1%)	dog	dog	dog

Table 2: Example figures and KL-score, Z-score characterization

with configuration MA3 (2) (a model with 1024 flattened values from Conv2D layers – layer 6, 128 dense neurons – layer 7 with ReLU activations). Figure 1 provides boxplot [20] based visualizations (one for each of the 10 classes) of some representative dense neurons in layer 7, and Figure 2 provides a histogram plot of the number of hidden units that fire for distinct classes (for both layer 6 & 7).

We make the following observations. hidden unit number 1 (Figure 1a) generates a wide range of activation values for the 9th class, but has activation values very close to 0 for the 1st, 2nd & 10th classes. On a similar note, hidden-unit 128 (the middle neuron in th layer, illustrated in Figure 1c) shows a unique pattern for the activation value distribution for the 3rd class. On the other hand, hidden unit 65 (Figure 1b) effectively does not generate non-zero activation values for 6 output classes. From similar analysis performed with both MNIST and CIFAR10 datasets, we observe that: (a) hidden unit activations typically possess a unique distributional pattern for one or more classes and (b) the distributions are not necessarily normal. These unique patterns might help in both discriminating among classes and in quantifying uncertainty–e.g., if the activation value of hidden-unit 1 for an unknown test instance (that has been declared to be the 9th class by the softmax output) is, say, 15.0 rather than 5.1 (closer to the mean of 9th class), the DNN is likely to be more uncertain of this classification. Our plots clearly show that distributions are not typically normal. In addition, Figure 2 plots the histogram (percentage) of hidden units, as a function of the number of distinct classes that activate each hidden unit at least once. We see that, across both layers 6 and 7, the dominant majority of hidden units are fired by three or fewer of the 10 classes. This result provides further evidence that most hidden units have distinct *class-dependent* activation patterns, lending further credence to our exploration of PADs as a means for identifying class labels for test samples.

3.2 Characterizing KL-score and Z-Score

In this section, we evaluate the characteristics of KL-divergence and Z-score based values obtained for several images from MNIST and CIFAR10 datasets using MA3 & CA1 configurations (Table 1 & 4), respectively. Table 2 shows different KL and Z-score values, as well as the output of the softmax layer, the classes corresponding to the minimum KL and Z-scores and the ground truth, for 4 different representative images (2 for MNIST, 2 for CIFAR10) illustrated in Figure 3.

In the MNIST sample (ground truth=6) in Figure 3a, the minimum KL score (1.073) and Z-score (0.594) for this sample (plotted in Table 2) correspond to the correct class “6”. In this case, the softmax output, the minimum KL-score and the minimum Z-score label all agree and are correct. In contrast, for Figure 3b, the class with the minimum KL and Z-score is 9 (agreeing with the ground truth), whereas softmax output suggests the class 5. In this case, the PAD-related features provide a correct classification while the output softmax does not. Figure 3c depicts an interesting example where the two top softmax output candidates (“ship” with 76.5% confidence and “truck” with 18.8% confidence) are both incorrect. However, the KL and Z-score metrics provide “automobile” (the correct inference) and “truck” respectively. Further, in Figure 3d, the softmax layer outputs the class “truck” (confidence> 73.1%), whereas the KL and/or Z-scores correctly indicate that the output should be “dog”. While we defer the presentation of comprehensive results on overall accuracy till Section 4, the examples presented here do attest to the discriminative potential of PADs.

4 Experimental Evaluation of PAD Performance

In this section, we empirically show that PADs can be used for a variety of uses, ranging from uncertainty quantification to ensuring highly accurate inferences.

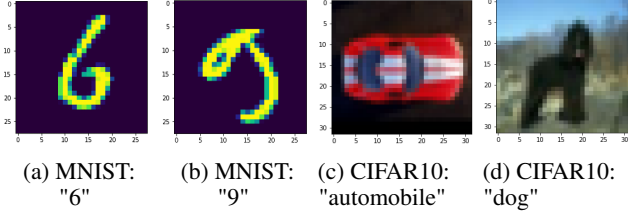


Figure 4: Example from Modified-MNIST dataset

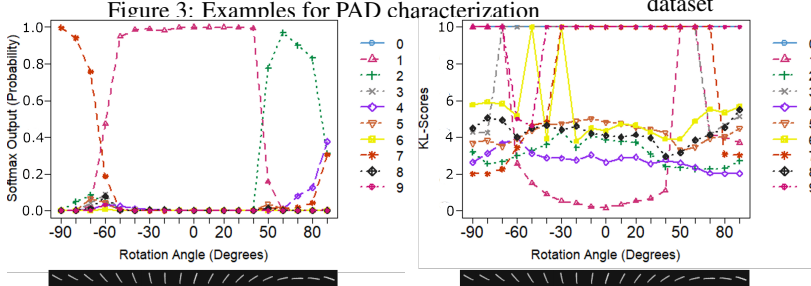


Figure 5: Softmax (MA1 model): Rotational MNIST

Figure 6: KL-Score (MA1 model): Rotational MNIST

	MNIST	CIFAR-5
MC Dropout [13]	99.5 %	84 %
Deep Ensemble [24]	99.3 %	79 %
EDL [42]	99.3 %	83 %
Softmax	99.4 %	80 %
KL	99.1 %	79 %
Z-score	96.3 %	76 %

Table 3: Comparison of classification accuracies for MNIST and CIFAR-5 for uncertainty quantifying techniques using LeNet configuration in [29]

4.1 Using PADs for Uncertainty Quantification

In this section, we observe how uncertainty is quantified using PADs of hidden layer units. Similar to experiments carried out by Gal *et. al.* [13] and Sensoy *et. al.*[42], we carried out experiments using PADs (with several configurations) on MNIST images under varying degrees of rotation. Figures 5 and 6 show the softmax outputs and KL-scores obtained using the MA1 model (Table 1), using rotations on an original “1” sample. For rotation angles between $(-90^\circ, -65^\circ)$, both softmax output and KL-scores suggest that the output is in fact 7. But, the softmax output gives confidence values in excess of 75% (more than 90% for certain angles), which is over-optimistic given that the model was never trained for such images. Similar results were observed in Gal *et. al.*, where they obtain a distribution of softmax outputs using dropout. However, even the dropout-based technique (as well as prior Bayesian approaches) result in higher confidence values. The PAD-based approach (Figure 6), however provides a more conservative picture: while the class “7” does have the lowest KL-score, the KL-scores of other classes (e.g., “2” & “4”) are quite similar, indicating that the DNN is not very confident of its inference. Similar results hold for rotation angles between $(50^\circ, 90^\circ)$, where the softmax output continues to have a misleadingly high confidence ($>75\%$). However, in the “normal range” of $(-40^\circ, 40^\circ)$, the KL-score for the correct class (“1”) is *significantly lower* than that of other classes, indicating that the DNN has low inferring uncertainty. In addition, we see that the PAD-based KL-score is able to offer a *finer-grained* measure for uncertainty, with the KL-score for “1” increasing gradually, even for 5° increments. In contrast, the softmax output remains high ($>96\%$ for all rotations between $(-60^\circ, 50^\circ)$). Further, Table 3 compares classification accuracies of models and techniques which quantify different types of uncertainty (it should be noted that the purpose of these techniques is not to have high accuracies per se, but to have reliable uncertainty estimates).

4.2 Using PADs for Inference

We now show how the discriminative capabilities of KL-score and Z-score values (illustrated in Section 3.2) can help improve the inferring process. To compare with the baseline approach (based on the softmax output layer), we consider several alternative PAD-based inferring strategies which operate on the hidden-layer activation values: *KL* and *Z-score* approaches output the class with the lowest KL-Score and Z-score, respectively; *EnsAND* generates a class label only when all 3 measures (softmax, KL, Z-score) unambiguously agree on the same class; while *EnsOPT* serves as an alternative optimal (*oracular*) baseline that picks the correct class if at least one of the 3 approaches (softmax, KL, Z-score) is correct.

Table 4 plots the classification accuracy of these approaches (for different datasets and models). We see that PAD-based *KL* and *Z-score* accuracy comparable to the softmax baseline, especially when applied to neural activations in the latter (deeper) part of the DNN. Further, an optimal ensemble technique *EnsOPT*, which smartly combines the PAD and softmax output inferences, can in fact

Reference (Table 1)	Layer	Accuracy				
		Softmax	KL	Zscore	EnsAND	EnsOPT
MA1	128-Dense Layer	99.03%	98.40%	98.27%	97.88%	99.34%
MA2	128-Dense Layer	99.44%	99.17%	99.04%	98.82%	99.59%
MA3	128-Dense Layer	99.56%	99.31%	99.15%	99.08%	99.66%
CA1	512-Dense Layer	88.17%	88.11%	88.24%	86.85%	89.63%
CA2	2048-Flattened Value Layer (24 th Layer)	89.31%	84.11%	84.05%	79.25%	92.95%
CA3	Average Pooling Layer	92.75%	89.11%	85.74%	78.31%	94.97%
FMA1	256-Dense Layer	91.81%	91.22%	91.32%	89.77%	93.23%

Table 4: Comparison of accuracy for different model architectures and datasets

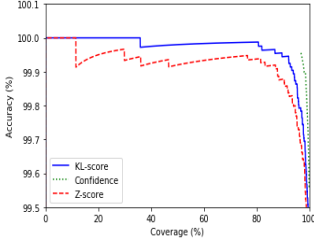


Figure 7: MNIST (MA3): Coverage vs. Accuracy

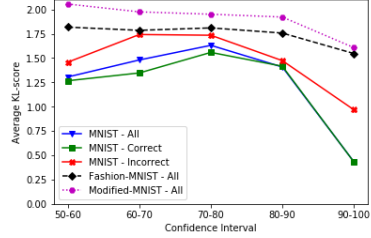


Figure 8: MNIST (MA3): KL-score vs. softmax confidence values, for MNIST & different OOD data. (notMNIST values outside plotted range)

Dataset	S1	S2	S3
notMNIST	100.00%	99.98%	99.98%
Fashion-MNIST	79.77%	97.69%	79.27%
Modified-MNIST	41.74%	98.32%	41.71%
MNIST	00.68%	15.36%	00.89%

Table 5: MA3: Rejection Rate for OOD vs. in-Distribution data for 3 different strategies. (Ideally, OOD rejection rate=100%.)

exceed baseline accuracy, at least for the MNIST, CIFAR10 and Fashion-MNIST benchmark datasets. We additionally considered configurations CA2, CA3 and observed that PAD-based accuracy increases as we go deeper in the network³—for example, in CA2, Z-score based accuracy was 53.1%, 69.4%, 83.45%, 84.05% for convolutional layers numbered 12,17,20 and 24 respectively. This result is consistent with prior work (Section 5) which demonstrates that deeper layers of a DNN are able to capture more specific features. While we omit results due to space limitations, we also tested PAD-based inferencing using other types of hidden layer—e.g., flattened values in CA2, pooling layers in CA3, etc., as well as when different regularization techniques (e.g., Data Augmentation, Dropout, Batch Normalization) were used. The results are consistent: PAD-based classification provides high accuracy under partial computation in all cases, demonstrating the *versatility* of this representation.

As a final illustration of using PAD in inferencing, we consider the use of DNNs in mission-critical scenarios, where we desire that automated DNN classification should have ‘near-100%’ accuracy—i.e., it should aggressively refer *uncertain* test samples to explicit manual verification. (An example would be DNNs used in medical image analysis) There is clearly a tradeoff between *coverage* (the percentage of samples that the DNN automatically classifies) and *accuracy* (defined over the *covered* samples). We compare three alternatives in terms of this tradeoff: (a) baseline, which uses the softmax *confidence* value to quantify uncertainty and thus invokes manual intervention when this confidence falls below a threshold; (b) KL-score and (c) Z-score, both of which invoke manual intervention when the corresponding metric exceeds a specified threshold. Figure 7 plots the resulting accuracy vs. coverage tradeoff. We see that the KL-score approach is able to explore this tradeoff continuum—e.g., it can ensure over 99.99% accuracy by filtering out around 20% of the test samples for manual inspection. In contrast, while the baseline softmax approach does have high initial accuracy, it cannot easily push the accuracy higher as confidence does not reliably indicate uncertainty.

4.3 Using PADs to identify out-of-distribution data

Given PAD’s intrinsic characterization of the *typical* neural activity for each class, we now demonstrate its use in reliably identifying *out-of-distribution data* (OOD). We used *Fashion-MNIST*, *notMNIST* and *Modified-MNIST* as exemplars of OOD data, injecting their samples into model MA3 (Table 1) that has been trained on the MNIST dataset. For the in-distribution MNIST data, Figure 8 plots the average KL-score values for samples, categorized by the confidence value produced at the output (softmax) layer. Plots are generated separately for the entire MNIST dataset (MNIST-All), as well as the test samples that are correctly or incorrectly classified (MNIST-Correct & MNIST-

³CA2 configuration used flattened values (24th layer), activation matrices of conv2d layers (12th, 17th and 20th layers) to formulate PADs while CA3’s pooling layers were used. In CA2, Conv2D layers are of the shapes (8,8,128), (16,16,64) and had 8192, 16384 individual values which we considered as hidden units to create PADs for layers in the middle of the network.

Incorrect, respectively). We see that even when the classifier is highly confident (confidence values $\in \{90, 100\}\%$), the KL-score for incorrect samples is more than double (0.97) that of comparable correct samples. Clearly, high KL-scores can help identify incorrect classification attempts.

This trend is further borne out when MA3 is used to classify OOD samples. For both Fashion-MNIST and Modified-MNIST samples, the average KL-score is 3-4 times larger than that obtained for in-distribution samples, even though many OOD samples are associated with high softmax confidence values. To further quantify this, we evaluate 3 different OOD-identification strategies: (i) *S1*: this filters out samples whose softmax confidence is below a threshold α ($=0.95$ in the MNIST experiments); (ii) *S2*: this PAD-based strategy filters out samples whose KL-score exceeds a threshold β ($=0.65$ in our experiments), and (iii) *S3*: this hybrid strategy filters out only those samples whose $confidence < \alpha$ AND $KL - score \geq \beta$. Table 5 plots the percentage of rejected samples for all 3 strategies. We see that the pure confidence-based *S1* strategy is effective only when the data is completely different (notMNIST), but performs poorly (rejection rate $\sim 40\%$) when the OOD dataset has some similarities (Modified-MNIST). In contrast, strategy *S2* can reject the vast majority of OOD samples, but at the cost of a higher rejection rate for in-distribution (MNIST) samples. By combining both predicates, strategy *S3* achieves both higher OOD and low in-distribution rejection rates.

5 Related Work

Hidden-Layers of Deep Neural Networks: Researchers have explored the interpretability of Convolutional Neural Networks (CNNs) by analyzing their hidden layers [51, 52]. They have suggested that DNNs tend to learn general features such as Gabon filters or Color blobs in the first few layers, while deeper layers learn more dataset-specific features. In an interesting study, Alain & Bengio [1] discuss the possibility of creating separately trained linear classifiers aka "probes" using parameters of hidden layers. Similar to our study, they reported that linear separability (and thus classification accuracy) increases as we go deeper in the network. However, their approach requires training a separate classifiers. Another study [3] proposes using the alignment of individual hidden units of a CNN to quantify model interpretability. [40] studies class specific information in hidden layers of CNNs using Singular Vector Canonical Correlation Analysis (SVCCA). Our methodology has conceptual overlap with [5, 40, 1]. However, we believe that PAD provides a novel, generalized construct with multiple uses (unlike [1] – focused purely on classification inference) and defines useful statistical measures on the underlying activation distributions.

Model Pruning: Researchers have proposed different model pruning strategies (e.g., [25, 50, 33, 2]) that utilize various properties of hidden layers –e.g., weight-based pruning of convolutional filters or entire nodes. PAD, on the other hand, models a neuron’s activation values on a per-class basis, and applies statistical aggregation across multiple neurons, as a means to identify class-specific activation patterns.

Uncertainty in DNNs: Bayesian Neural Networks have been discussed thoroughly in literature as a mathematically grounded way of modelling neural network uncertainty [34, 47, 30]. Recently, there has been a shift towards modelling uncertainty using Bayesian Inference [18, 36]. Variational Inference (VI) based Bayesian techniques have been proposed [17, 15] even though their validity has been questioned in subsequent research [41, 37]. Such Bayesian techniques have higher computational complexity, in both training and inference, and are not yet fully supported in mainstream deep learning libraries. Gal *et. al.* [11, 13] have suggested that Dropout [44] can be utilized to provide Bayesian approximations in DNNs. An alternative technique based on batch normalization was proposed by Teye *et. al.* [45] which has similar traits to that of [13]. Both these techniques rely on a specific regularization technique (both batch normalization & dropout in CNNs have associated problems [12, 43, 48]). They also require multiple stochastic passes (using the same test sample) to derive an uncertainty measures and are thus not suitable for real-time applications. An ensemble approach for non-Bayesian uncertainty modelling, proposed in [24], requires the use of several DNNs for both training and inferencing. Another interesting work, [42] employs Dempster-Shafer theory (a generalization of bayesian logic [14]) to model uncertainty by adding an additional “uncertainty class” to the output layer–this method requires changes in training (including loss function and logits). In contrast to several of these approaches, PADs requires no modifications to training, does not employ an explicit Bayesian framework and instead uses low dimensional statistics over the activation values of hidden layer units to distinguish between classes.

6 Conclusion

We have proposed a novel and intuitive technique, called PAD, to capture class separability in DNNs using the activation values of hidden layer units. Intuitively, PAD leverages on the collective cross-class discrimination capability of all neurons in a hidden layer, provides greater expressivity than available purely at the output layer. As exemplars of PAD’s utility, we have demonstrated its use for (a) capturing predictive uncertainty in classification; (b) obtaining highly accurate inferences early, without fully executing a DNN; and (c) filtering out out-of-distribution samples.

We believe that PADs provide a promising representation that can form the basis for interesting future work. For example, (a) PADs may need to be modified to be applicable to other tasks (e.g., regression) beyond just classification, and (b) PADs may provide a mechanism for *class-aware* model compression & pruning (e.g., by selectively discarding neurons that fire across multiple classes and thus are less discriminative).

References

- [1] Guillaume Alain and Yoshua Bengio. 2017. Understanding intermediate layers using linear classifier probes. *ICLR (Workshop)* (2017).
- [2] Sajid Anwar, Kyuyeon Hwang, and Wonyong Sung. 2017. Structured Pruning of Deep Convolutional Neural Networks. *ACM Journal on Emerging Technologies in Computing Systems (JETC)* (2017).
- [3] David Bau, Bolei Zhou, Aditya Khosla, Aude Oliva, and Antonio Torralba. 2017. Network Dissection: Quantifying Interpretability of Deep Visual Representations. *CVPR* (2017).
- [4] Yaroslav Bulatov. 2011. notMNIST dataset. (2011). <http://yaroslavvb.blogspot.com/2011/09/notmnist-dataset.html>
- [5] Ian E.H. Yen Pradeep Ravikumar Chih-Kuan Yeh, Joon Sik Kim. 2018. Representer Point Selection for Explaining Deep Neural Networks. *NIPS* (2018).
- [6] François Chollet et al. 2015. Keras. <https://github.com/fchollet/keras>. (2015).
- [7] François Chollet et al. 2019. CIFAR10 Sample Code - Keras Code Examples GitHub Repository. (2019). https://github.com/keras-team/keras/blob/master/examples/cifar10_cnn.py
- [8] François Chollet et al. 2019. MNIST Sample Code - Keras Code Examples GitHub Repository. (2019). https://github.com/keras-team/keras/blob/master/examples/mnist_cnn.py
- [9] Yann Duan, Xi Chen, Rein Houthoofd, John Schulman, and Peiter Abbeel. 2016. Benchmarking Deep Reinforcement Learning for Continuous Control. In *33rd International Conference on Machine Learning (ICML)*.
- [10] Martín Abadi et al. 2015. TensorFlow: Large-Scale Machine Learning on Heterogeneous Systems. (2015). <http://tensorflow.org/> Software available from tensorflow.org.
- [11] Yarin Gal. 2016. Uncertainty in Deep Learning. *PhD Thesis* (2016).
- [12] Yarin Gal and Zoubin Ghahramani. 2016. Bayesian Convolutional Neural Networks with Bernoulli Approximate Variational Inference. *ICLR* (2016).
- [13] Yarin Gal and Zoubin Ghahramani. 2016. Dropout as a Bayesian Approximation: Representing Model Uncertainty in Deep Learning. *International Conference on Machine Learning (ICML)* (2016).
- [14] Jean Gordon and Edward H. Shortliffe. 1984. The Dempster-Shafer Theory of Evidence. *Rule-Based Expert Systems: The MYCIN* (1984).
- [15] A Graves. 2011. Practical variational inference for neural networks. *NIPS* (2011).

- [16] Kaiming He, Xiangyu Zhang, Shaoqing Ren, and Jian Sun. 2015. Deep Residual Learning for Image Recognition. *arXiv preprint arXiv:1512.03385* (2015).
- [17] J M Hernandez-Lobato and R P Adams. 2015. Probabilistic backpropagation for scalable learning of bayesian neural networks. *ICML* (2015).
- [18] S Herzog and D. Ostwald. 2013. Experimental biology: Sometimes Bayesian statistics are better. *Nature* 494 (2013).
- [19] H.N.Io and C.B.Lee. 2017. Chatbots and conversational agents: A bibliometric analysis. *International Conference on Industrial Engineering and Engineering Management (IEEM)* (2017), 215–219. <https://doi.org/10.1109/IEEM.2017.8289883>
- [20] J. D. Hunter. 2007. Matplotlib: A 2D graphics environment. *Computing In Science & Engineering* 9, 3 (2007), 90–95. <https://doi.org/10.1109/MCSE.2007.55>
- [21] Alex Krizhevsky. 2009. Learning Multiple Layers of Features from Tiny Images. (2009). <https://www.cs.toronto.edu/~kriz/cifar.html>
- [22] Abhijeet Kumar. 2018. Achieving 90% accuracy in Object Recognition Task on CIFAR-10 Dataset with Keras: Convolutional Neural Networks. *Applied Machine Learning Blog* (2018). <http://tiny.cc/c4os6y>
- [23] AiOTA LABS. 2019. Quantifying Accuracy and SoftMax Prediction Confidence For Making Safe and Reliable Deep Neural Network Based AI System. *UseJournal* (2019).
- [24] Balaji Lakshminarayanan, Alexander Pritzel, and Charles Blundell. 2017. Simple and Scalable Predictive Uncertainty Estimation using Deep Ensembles. *31st Conference on Neural Information Processing Systems (NIPS)* (2017).
- [25] Yann LeCun, John S. Denker, and Sara A. Solla. 1990. Optimal Brain Damage. In *Advances in Neural Information Processing Systems 2*, D. S. Touretzky (Ed.). Morgan-Kaufmann, 598–605. <http://papers.nips.cc/paper/250-optimal-brain-damage.pdf>
- [26] Yann Lecunn, Yoshua Bengio, and Geoffrey Hinton. 2015. Deep Learning. *Nature* 521 (2015), 436–444.
- [27] Y. LeCunn, L. Bottou, Y. Bengio, and P. Haffner. 1998. Gradient-based learning applied to document recognition. *Proc. IEEE* (1998).
- [28] Geert Litjens, Thijs Kooi, Babak Ehteshami Bejnordi, Arnaud Arindra Adiyoso Setio, Francesco Ciompi, Mohsen Ghafoorian, Jeroen A.W.M. van der Laak, Bram van Ginneken, and Clara I. Sánchez. 2017. A survey on deep learning in medical image analysis. *Medical Image Analysis* 42 (2017), 60 – 88. <https://doi.org/10.1016/j.media.2017.07.005>
- [29] C. Louizos and M. Welling. 2017. Multiplicative normalizing flows for variational bayesian neural networks. *ICML* (2017).
- [30] David JC MacKay. 1992. A practical Bayesian framework for backpropagation networks. *Neural computation* 4(3) (1992), 448–472.
- [31] David JC MacKay. 1995. Probable networks and plausible predictions—a review of practical Bayesian methods for supervised neural networks. *Network: Computation in Neural Systems* 6(3) (1995), 469–505.
- [32] Margaret Maynard-Reid. 2018. Fashion-MNIST with tf.Keras. (2018).
- [33] Pavlo Molchanov, Stephen Tyree, Tero Karras, Timo Aila, and Jan Kautz. 2017. Pruning Convolutional Neural Networks for Resource Efficient Inference. *ICLR* (2017).
- [34] R M. Neal. 1995. Bayesian learning for neural networks. *PhD thesis, University of Toronto* (1995).

- [35] Anh Nguyen, Jason Yosinski, and Jeff Clune. 2015. Deep Neural Networks are Easily Fooled: High Confidence Predictions for Unrecognizable Images. *Conference on Computer Vision and Pattern Recognition (CVPR)* (2015).
- [36] Regina Nuzzo. 2013. Statistical Errors. *Nature* 506(13) (2013), 150–152.
- [37] I. Osband, J. Aslanides, and A. Cassirer. 2018. Randomized Prior Functions for Deep Reinforcement Learning. *32nd Conference on Neural Information Processing Systems (NIPS)* (2018).
- [38] Manajit Pal. 2019. Deep Learning for Self-Driving Cars. *Towards Data Science* (2019).
- [39] Larrel Pinto and Abhinav Gupta. 2016. Supersizing self-supervision: Learning to grasp from 50K tries and 700 robot hours. *IEEE International Conference on Robotics and Automation (ICRA)*, 3406–3413.
- [40] Maithra Raghu, Justin Gilmer, Jason Yosinski, and Jascha Sohl-Dickstein. 2017. SVCCA: Singular Vector Canonical Correlation Analysis for Deep Learning Dynamics and Interpretability. *Advances in neural information processing systems(NIPS)* (2017).
- [41] H. Ritter, A. Botev, and D. Barber. 2018. A scalable laplace approximation for Neural Networks. *ICLR* (2018).
- [42] Murat Sensoy, Lance Kaplan, and Melih Kandemir. 2018. Evidential Deep Learning to Quantify Classification Uncertainty. *32nd Conference on Neural Information Processing Systems (NeurIPS)* (2018).
- [43] Jost Tobias Springenberg, Alexey Dosovitskiy, Thomas Brox, and Martin Riedmiller. 2015. Striving for Simplicity: The All Convolutional Net. *ICLR Workshop* (2015).
- [44] N. Srivastava, G. Hinton, A. rizhevsky, I. Sutskever, and R. Salakhutdinov. 2014. Dropout: A simple way to prevent neural networks from overfitting. *The Journal of Machine Learning Research* (2014).
- [45] Mattias Teye, Hossein Azizpour, and Kevin Smith. 2018. Bayesian Uncertainty Estimation for Batch Normalized Deep Networks. *International Conference on Machine Learning (ICML)* (2018).
- [46] G. van Rossum. 1995. *Python tutorial*. Technical Report CS-R9526. Centrum voor Wiskunde en Informatica (CWI), Amsterdam. Software available from python.org.
- [47] C. K. I. Williams. 1997. Computing with infinite networks. *NIPS* (1997).
- [48] Xiaolin Hu Jian Yang Xiang Li, Shuo Chen. 2018. Understanding the Disharmony between Dropout and Batch Normalization by Variance Shift. *arXiv:1801.05134* (2018).
- [49] Han Xiao, Kashif Rasul, and Roland Vollgraf. 2017. Fashion-MNIST: a Novel Image Dataset for Benchmarking Machine Learning Algorithms. (2017). arXiv:cs.LG/1708.07747
- [50] Shuochao Yao, Yiran Zhao, Aston Zhang, Lu Su, and Tarek Abdelzaher. 2017. DeepIoT: Compressing Deep Neural Network Structures for Sensing Systems with a Compressor-Critic Framework. *SenSys* (2017).
- [51] J. Yosinski, J. Clune, Y. Bengio, and H. Lipson. 2014. How transferable are features in deep neural networks? *Advances in neural information processing systems(NIPS)* (2014), 3320–3328.
- [52] M. D. Zeiler and R Fergus. 2014. Visualizing and understanding convolutional networks. *European conference on computer vision (ECCV)* (2014), 818–833.